Miner Deposita (2006) 41:821–835
DOI 10.1007/s00126-006-0093-3

LETTER

Direct evidence of fluid mixing in the formation of stratabound Pb–Zn–Ba–F mineralisation in the Alston Block, North Pennine Orefield (England)

Jon E. Bouch · Jonathan Naden · Thomas J. Shepherd · John A. McKervey · Brian Young · Antony J. Benham · Hilary J. Sloane

Received: 21 July 2006 / Accepted: 24 August 2006 / Published online: 10 October 2006

Abstract The North Pennine Orefield Alston Block has produced approximately 4 Mt Pb, 0.3 Mt Zn, 2.1 Mt fluorite, 1.5 Mt barite, 1 Mt witherite, plus a substantial amount of iron ore and copper ore from predominantly vein-hosted mineralisation in Carboniferous limestones. However, a significant proportion of this production (ca. 20%) came from stratabound deposits. Though much is known about the vein mineralisation, the relationship between the veins and the stratabound mineralisation is not well-understood. New petrographic, isotopic and fluid inclusion data derived from samples of stratabound mineralisation allow us to present a unified model that addresses the genesis of both the vein and stratabound styles of mineralisation. The mineralisation can be considered in terms of three episodes:

1. *Dolomitisation and ankeritisation* Limestones in the vicinity of the stratabound mineralisation were pervasively dolomitised/ankeritised, and developed vuggy porosity in the presence of a high-salinity brine consistent with fluids derived from adjacent mud and shale-filled basins.
2. *Main stage fluorite–quartz–sulphide mineralisation* Metasomatism of limestone was accompanied by brecciation, dissolution and hydrothermal karstification with modification of the existing pore system. The open space was filled with fluorite, galena, sphalerite, quartz and barite, formed in response to mixing of low-salinity sodic groundwater with high-salinity calcic brine with elevated metal contents (particularly Fe up to 7,000 ppm) relative to "normal" high total dissolved solids sedimentary brines.
3. *Late-stage barite mineralisation* paragenetically appears to represent either the waning stages or the distal portions of the main hydrothermal circulation system under cooler conditions.

Keywords North Pennine Orefield · Alston Block · Stratabound mineralisation

Editorial handling: B. Lehmann

J. E. Bouch (✉) · J. Naden · J. A. McKervey · A. J. Benham
British Geological Survey, Kingsley Dunham Centre,
Nicker Hill, Keyworth,
NG12 5GG Nottingham, UK
e-mail: jbouch@bgs.ac.uk

T. J. Shepherd
School of Earth Sciences, University of Leeds,
LS2 9JT Leeds, UK

B. Young
British Geological Survey,
Murchison House, West Mains Road,
EH9 3LA Edinburgh, UK

H. J. Sloane
Natural Environment Research Council Isotope
Geosciences Laboratory, Kingsley Dunham Centre,
Nicker Hill, Keyworth,
NG12 5GG Nottingham, UK

Present address:
B. Young
Department of Earth Sciences,
University of Durham, Science Laboratories,
South Road,
Durham, DH1 3LE, UK

Introduction

The North Pennine Orefield (NPO; Fig. 1) of the Alston Block is a fluoritic sub-type of Mississippi Valley-type deposits akin to deposits in Kentucky and Illinois in North

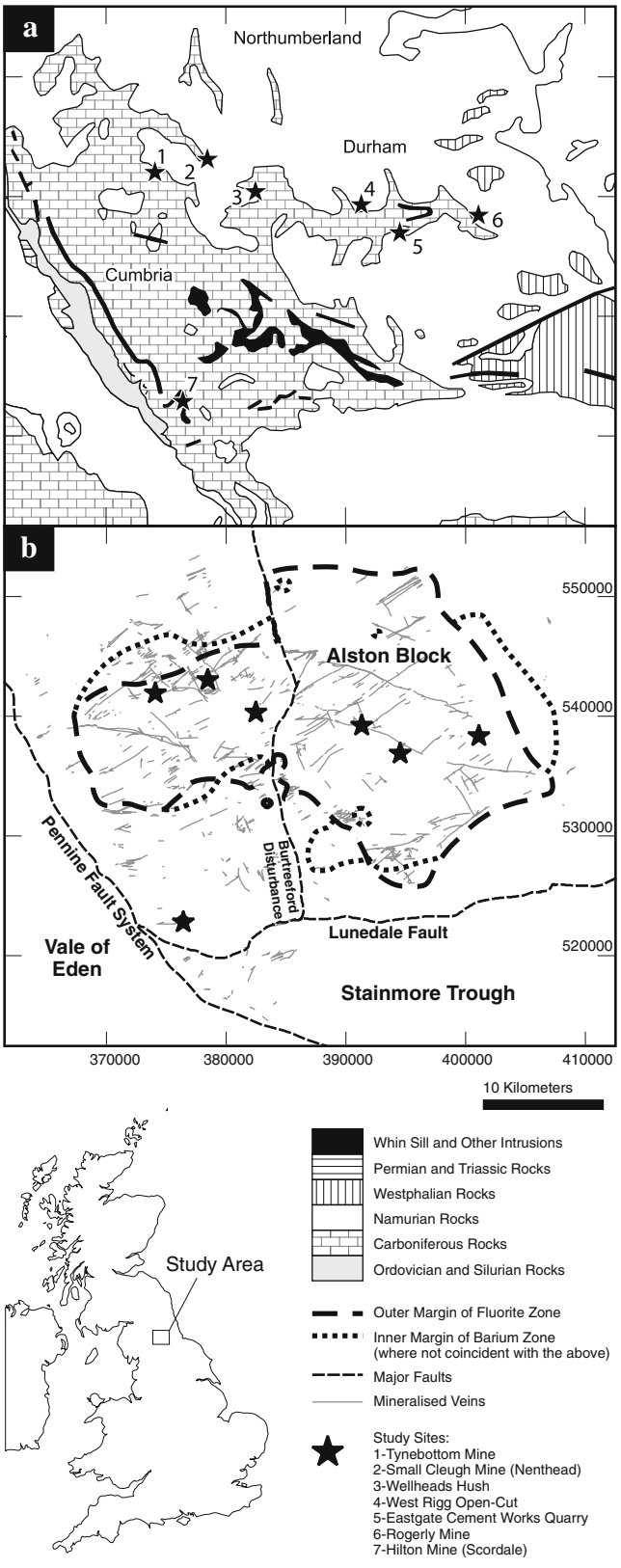

Fig. 1 The location, structure and geology of the North Pennine Orefield. **a** Generalised geology of the study area, along with the positions of the studied deposits. **b** Main structural elements and the positions of the mineralised veins in the area

America (Dunham 1990; Plant et al. 1995) and is estimated to have produced approximately 4 Mt lead, 0.3 Mt zinc, 2.1 Mt fluorite, 1.5 Mt barite, 1 Mt witherite, plus a substantial amount of iron ore and a few hundred tonnes of copper ore. Previous ore genesis studies have focussed on the dominant vein-style mineralisation. However, significant ore (1.7 Mt of iron ore plus lead, zinc, fluorite, barite and witherite) was also worked from limestone-hosted stratabound mineral deposits, which are thought to represent metasomatic replacement adjacent to the veins (Dunham 1990), but have attracted relatively little research interest.

In this paper we provide a unified model that addresses the genesis of both the vein and stratabound styles of mineralisation. In particular, we demonstrate that in addition to simple metasomatism, the stratabound mineralisation results from significant fracturing, brecciation, host-rock dissolution and hydrothermal karstification both before and during the main mineralisation. New stable isotope ($\delta^{13}C$ and $\delta^{18}O$ on carbonates) and fluid inclusion microthermometric and microchemical data show that mixing of fluids from multiple sources plays an important role in the genesis of the stratabound mineralisation, which is co-genetic with the main vein-style mineralisation. The microchemical data also show that the fluids had highly elevated metal, particularly Fe, contents relative to normal high total dissolved solids (TDS) sedimentary brines.

Geological setting

The NPO is located within the structural highs of the Alston and Askrigg blocks (Dunham and Wilson 1985; Dunham 1990). In this study, we focus on the deposits of the Alston Block, which comprise Lower Palaeozoic sedimentary and volcanic rocks intruded by Caledonian granites, and overlain by up to ca. 600 m of mainly cyclothemic sequences of Carboniferous limestones, sandstones, mudstones and minor coals (Fig. 1).

The mineralisation occurs in dome-shaped zones related to the form of the underlying Weardale Granite. Within a central zone, both veins and stratabound ore bodies are dominated by abundant fluorite. Local centres of copper-rich mineralisation, in places accompanied by some bismuth, rare earth element minerals, and cassiterite have also been identified in this zone (Ixer 1986; Ixer et al. 1996; Ixer and Flowers, personal communication in Dunham 1990). Fluorite-bearing veins locally pass downwards into deeper zones dominated by quartz and iron sulphides. The fluorite zone is surrounded by an outer zone in which barium minerals [barite, witherite and $BaCa(CO_3)_2$ polymorphs] dominate. The transition from the fluorite to the barium zone is sharp, and coexisting fluorite and barium minerals are rare.

The vein mineralisation is hosted in a conjugate system of steeply dipping normal faults, with displacements typically of only a few metres. Veins are best developed in more competent lithologies (i.e. limestone) and fills comprise variably continuous mineral bands sub-parallel to the vein walls, commonly with open vugs in the centres of veins. Numerous, often repetitious, mineral bands are present, making the establishment of a general paragenetic sequence difficult. In the central fluorite zone, vein mineralisation is generally regarded as having formed from hot (up to 200°C) metal-rich saline brines (Sawkins 1966; Smith 1974; Moore 1980; Cann and Banks 2001), with cooler temperatures (<130°C) towards the margins (Sawkins 1966). The mineralising fluids are understood to be predominantly high salinity NaCl–$CaCl_2$ brines (typically about 20 wt% NaCl equivalent) and enriched in K and Li relative to oilfield brines (Rankin and Graham 1988; Cann and Banks 2001). Mineralisation temperatures and salinities are lower in the surrounding barium zone (<120°C and ~15 wt% NaCl equivalent; Cann and Banks 2001), and Dunham (1990) suggested that much of the barite may have formed at temperatures <70°C. Current models for mineralisation in the NPO typically invoke sulphide and fluorite precipitation in response to mixing of a metalliferous Cl-dominated brine (of various potential sources), with a sulphate-dominated brine (e.g. Solomon et al. 1971, 1972; Dunham 1990; Crowley et al. 1997; Cann and Banks 2001).

The stratabound deposits have largely been removed by mining, although Dunham (1948, 1990) provides comprehensive observations. The deposits are most strongly developed at the vein intersections and are generally elongated parallel to the veining. However, they can also be lobate in plan. Contemporary mine records reveal several instances of extensive stratabound mineralisation in limestone overlain by impervious mudstone, whereas vein ore shoots were normal in situations where sandstones directly overlie the limestone. This implies a strong hydrological and lithological control to the mineralisation. Though the stratabound mineralisation is classed as metasomatic (Dunham 1990), field observations and historical mining accounts suggest a significant open-space component. Dunham (1990) advocated metasomatic replacement accompanied by the generation of large cavities and a variety of collapse breccias and that, locally, porosity generation during or before mineralisation was in the region of 30 to 50% by volume.

The mineralisation is considered to have been initiated shortly after or during the cooling of the Whin Sill (ca. 295 Ma; Fitch and Miller 1967; Young et al. 1985; Dunham 1990) and to have continued into the Permian. However, consideration of the available radiometric data (Dunham et al. 1968; Shepherd et al. 1982; Davison et al. 1992; Lenehan 1997) suggests that the main phase of mineralisation was restricted to the period between the latest Permian (ca. 250 to 260 Ma) and the end of the Triassic (ca. 210 Ma; Cann and Banks 2001).

Materials and methods

Mineralised samples were collected from stratabound mineralisation at seven sites (Fig. 1; Table 1) in the NPO. The studied deposits include some of the better known and most productive examples of their type, including the formerly economically important Smallcleugh and Hilton deposits. However, most of the largest and most productive areas of stratabound mineralisation (e.g. Boltsburn and Allenheads) are now inaccessible. Though it is possible to make use of contemporary records for comparative purposes, it is possible that our observations are not wholly representative of the mineralisation style.

Petrography Petrographic, fluid inclusion and mineral microchemical analyses were conducted on standard polished thin sections and fluid inclusion wafers using a variety of techniques. Cathodoluminescence (CL) observations were made using Technosyn 8200 Mark II apparatus. Backscattered electron scanning electron microscope analyses were conducted using a LEO 435VP microscope with Oxford Instruments ISIS300 energy dispersive X-ray analyser. Microchemical mapping and point analyses of carbonates were undertaken using a Cameca SX-50 electron microprobe (EPMA).

Fluid inclusion microthermometry Data were collected using a Linkam MDS600 heating–freezing system calibrated against synthetic fluid inclusions, using the general methodology outlined by Goldstein (2001) and references therein. For monophase inclusions, salinity was determined after cryogenically or thermally stretching the inclusion to induce vapour nucleation. The errors in determining homogenisation temperature (T_h), first melting/eutectic (T_{fm}), last ice-melting (T_{ice}) and hydrate melting (T_{hyd}) are typically ±5, ±0.2, ±5 and ±0.2°C respectively. Where paired T_{ice} and T_{hyd} were available, *CalcicBrine* (Naden 1996) was used to calculate salinities in terms of the system NaCl–$CaCl_2$–H_2O. In the absence of T_{hyd} data, salinities were calculated in terms of the system $NaCl_2$–H_2O for $T_{ice} \geq -21.3$°C and in the system $CaCl_2$–H_2O for $T_{ice} < -21.3$°C. No pressure corrections were applied to the T_h data. The samples were also screened using epifluorescence, which failed to reveal any hydrocarbon-bearing inclusions. The majority of inclusions analysed were of primary (n=241) origin, with fewer pseudo-secondary (n=45) and secondary (n=47) inclusions. Comparison of

Table 1 Summary features of the stratabound mineralisation present at the study sites

Site name (Grid reference, British National Grid)	Host limestone formation	Stratabound mineralisation
Tynebottom Mine (3739 5418)	Tynebottom Limestone	Fine-grained quartz and chalcedony with disseminated galena, marcasite and pyrite. Vugs are lined with quartz, calcite, ankerite and purple fluorite.
Smallcleugh Mine (3787 5430)	Great Limestone	Ankerite, siderite and some fine-grained silica, with zebra dolomites and vugs in the most intensely mineralised beds. Vugs are lined with ankerite accompanied by quartz, calcite, and ore minerals. Galena and sphalerite occur as coarsely crystalline lenses and bands, as well as crystallised masses within vugs.
Wellheads Hush (3825 5403)	Great Limestone	Ankerite, siderite with minor fluorite and galena.
West Rigg Open Cut (3911 5392)	Great Limestone	Limonitic ironstone, derived from the supergene alteration of primary carbonates (almost certainly siderite and ankerite).
Eastgate Cement Works (3947 5368)	Great Limestone	Ankerite, siderite and quartz dominate, accompanied by purple and green fluorite, galena, quartz and aragonite in vugs.
Rogerley Mine (4009 5384)	Great Limestone	Fine-grained silica and ankerite, with large (up to 1 m diameter) vugs lined with deep green fluorite. Many vugs contain clay, which either represent insoluble residues from limestone dissolution or, more likely, clay washed into the cavities from the surface during recent or Quaternary times.
Hilton Mine (3764 5228)	Melmerby Scar Limestone	The Whin Sill has metamorphosed limestone to marble and shale to a fine-grained hornfels. The altered limestone is replaced by granular crystalline fluorite, together with barite and galena. Much of the stratabound mineralisation accessible today appears to be concentrated within a thin hornfelsed shale, which overlies the Limestone and is in turn overlain by the lower contact of the Whin Sill. Here, hornfelsed shale breccia clasts are cemented by yellow fluorite, white barite and smaller quantities of coarsely crystalline galena.

data from the different fluid inclusion generations reveals no detectable systematic differences in character between the different types.

Fluid inclusion microchemistry Fluid inclusions were ablated with a Geolas Q Plus eximer laser (ArF, 193 nm) and the ablated material analysed using an Agilent 7500c quadrupole inductively coupled plasma mass spectrometer fitted with a dynamic reaction cell. The optical delivery system used is that described by Gunther et al. (1997a). The sample ablation cell has a volume of approximately 13 cm^3, and the ablated material was removed from the cell in a stream of He gas (0.68 l/min) and premixed with Ar (0.95 l/min) before introduction to the plasma. Calibration was carried out using a combination of NIST reference glasses SRM 610 and 612 and aqueous standards ablated directly through the walls of glass capillaries (Gunther et al. 1997b; Allan et al. 2006). Analytical precision for Li, Na and K is typically better than 15% RSD, whilst Mg, Cl, Ca, Mn, Fe, Cu, Zn, Sr, Ba and Pb are reproducible within 30% RSD. Accuracy for most elements is within 15% (Allan et al. 2006). Isotope masses (^{7}Li, ^{23}Na, ^{24}Mg, ^{35}Cl, ^{39}K, ^{44}Ca, ^{55}Mn, ^{57}Fe, ^{63}Cu, ^{66}Zn, ^{88}Sr, ^{137}Ba, ^{208}Pb) were selected so as to minimise potential interferences. Although ^{57}Fe is relatively interference-free, some of the analyses were carried out under conditions where the reaction cell was pressurised with 2.5 l/min H_2 to eliminate interference from the $^{40}Ar^{16}O^+$ dimer on the $^{56}Fe^+$ and high Ar-based backgrounds on $^{39}K^+$. The use of a hydrogen reaction cell also precluded the analysis of Li and Cl. Limits of detection (i.e. 3σ on background counts) vary according to inclusion mass (volume×concentration of analyte) but are generally 1 to 10^2 $\mu g/g^{-1}$ for most elements. For data interpretation, Na was used as the internal standard; the concentration of Na being estimated from independent microthermometric calculations. Data processing was undertaken using in-house software (SILLS written by Murray Allan, Dept. Earth Sciences, University of Leeds).

Carbonate stable isotope analysis Samples of carbonate were extracted using microdrills and analysed for $\delta^{18}O$ and $\delta^{13}C$ using a procedure based on the methodology of McCrea (1950). Calcites were reacted at 25.2°C (Friedman and O'Neil 1977) and dolomites and ankerites at 100°C (Rosenbaum and Sheppard 1986). Analyses were undertaken on a VG Optima dual-inlet gas source mass spectrometer. Each batch of unknowns was run with three primary standards with known values with respect to NBS-19. The resultant gas values were further adjusted using Craig's correction for small levels of ^{17}O isotopes. The values were normalised through the primary standard and corrected to the solid carbonate value using a fractionation factor to account for the incomplete liberation of the oxygen in phosphoric acid.

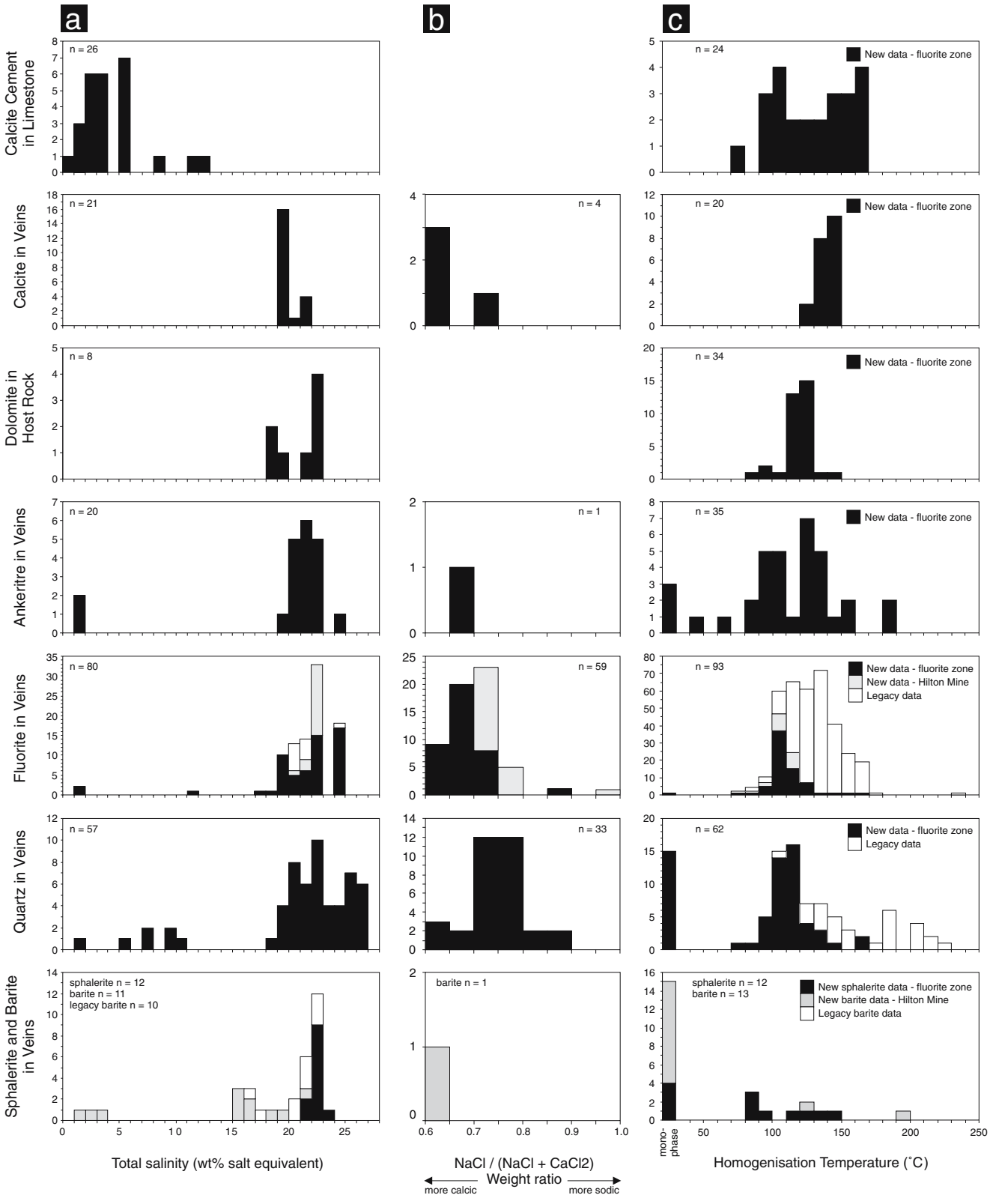

Fig. 2 Histograms of fluid inclusion microthermometric data for samples of stratabound mineralisation in the North Pennines, with analyses plotted according to mineral and paragenetic position. **a** Total salinity. **b** Relative proportions of Na and Ca as modelled using CalcicBrine (Naden 1996). **c** Homogenisation temperatures, including proportions of monophase inclusions. "Legacy data" from Smith (1974), Moore (1980), Christoula (1993) and Shepherd (unpublished data)

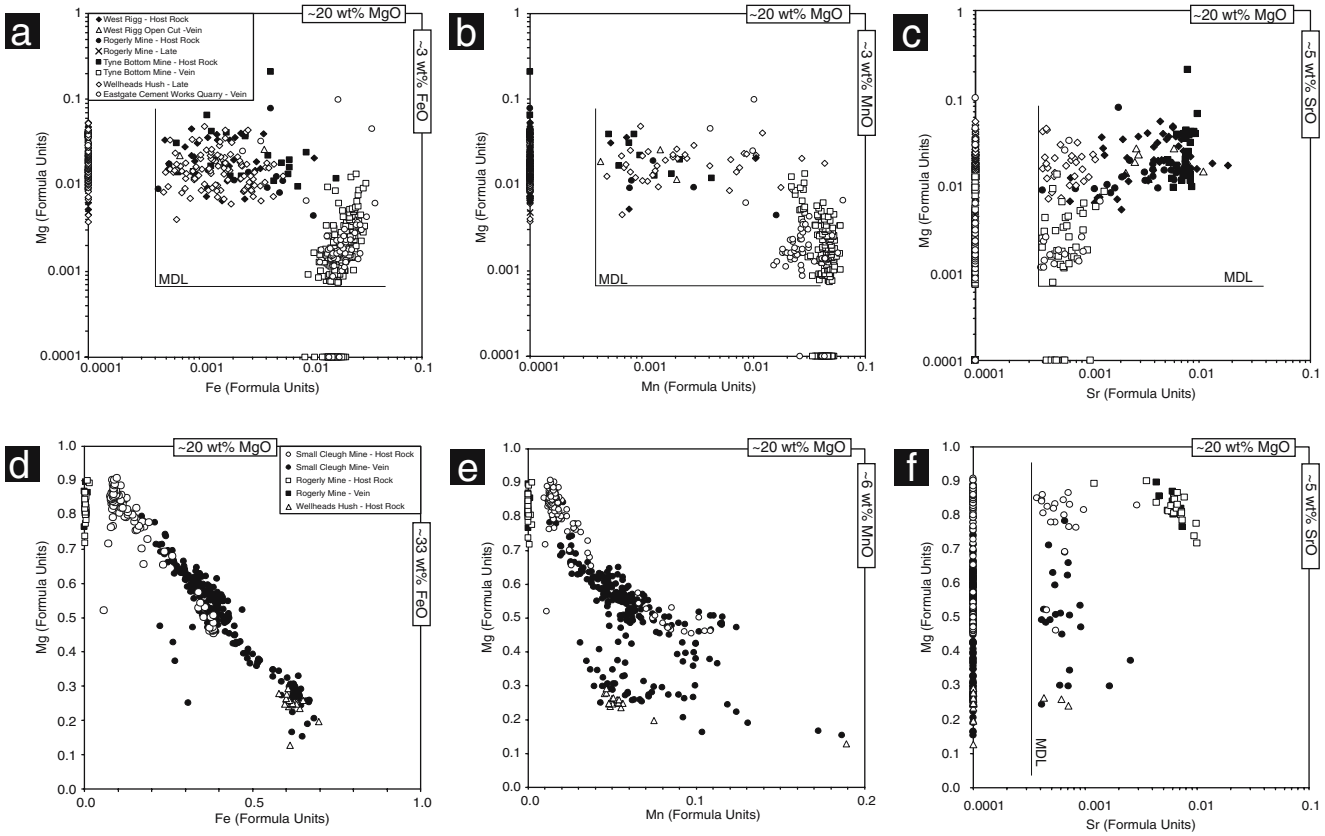

Fig. 3 Summary plots showing co-variations in carbonate composition as determined by EPMA for calcite (plots **a**, **b** and **c**) and dolomite/ankerite (plots **d**, **e** and **f**). All data are plotted as formula units, with carbonate compositions calculated on the basis of two cations. Estimated minimum detection limits are indicated, and points falling below these limits are displaced to nominal concentrations of 0.0001 formula units on the appropriate axes. In **d**, **e** and **f**, host rock dolomite/ankerite is plotted using *open symbols*, and fracture-lining/vug-lining dolomite is plotted using *filled symbols*. For all plots, approximate oxide wt% equivalents are quoted on the *X* and *Y* axes, and a linear relationship between concentrations expressed as formula units and oxide weight percent can be assumed for the purposes of approximation

Mineralisation history

Dolomitisation and ankeritisation

The undolomitised and unmineralised limestones do not contain any petrographical features consistent with marine diagenetic processes. However, fluid inclusions in calcite cements are of notably lower salinity (2 to 6 wt % salt equiv.; Fig. 2) than those observed within the paragenetically later dolomite/ankerite, fluorite and quartz, and the majority have T_{fm} (ca. −25°C) consistent with a NaCl-dominated fluid. This suggests that this fluid might represent slightly evolved seawater. CL and EPMA both indicate low Fe and Mn concentrations, but Sr concentrations in the calcite are high relative to later calcite veining (Fig. 3a–c). This signature was possibly inherited from precursor marine cements (Tucker and Wright 1990) and is consistent with a probable seawater derivation for this fluid. Whilst Mg contents are higher in the calcite cements relative to calcite related to later mineralisation, they are low (predominantly <0.5 wt% MgO) relative to marine diagenetic high Mg calcites that might be expected to contain several weight percent of MgO (Tucker and Wright 1990). Limited stable isotope data (n=4) from unaltered wall rock calcites indicate relatively light $\delta^{18}O$ compositions ($\delta^{18}O_{PDB}$ of −12.2 to −5.7‰; Table 2 and Fig. 4) compared with those from Carboniferous marine brachiopods ($\delta^{18}O$ typically between −3 and −8‰ PDB; Bruckschen and Veizer 1997). The presence of appreciable Sr, but the absence of textures indicative of marine diagenesis, suggests that later diagenetic processes have overprinted any marine diagenetic signatures. Fluid inclusion data suggest that this was probably due to interaction with slightly modified (concentrated) seawater, with slightly elevated temperatures during burial responsible for the lighter $\delta^{18}O$ signatures. The broad range of T_h for calcite cements (75 to 160°C; Fig. 2) may indicate some leakage of the inclusions in response to later heating during dolomitisation and mineralisation. The presence of some high salinity inclusions (up to 12 wt% salt equiv.) may also reflect overprinting by later fluids.

Table 2 Stable isotope data for samples from the North Pennines

Location	Mineral	Comment	Sample ID	$\delta^{18}O_{PDB}$ (‰)	$\delta^{13}C_{PDB}$ (‰)
Tyne Bottom Mine	Calcite	Limestone	NQ1033-01	−12.16	+1.51
		Vein calcite	NQ1033-02	−13.05	−3.42
Smallcleugh Mine	Dolomite	Grey dolostone	NQ1015-01	−9.92	−2.15
		Muddy dolostone	NQ1016-02	−7.27	+1.33
		Buff dolostone	NQ1016-03	−8.99	−0.44
		Grey dolostone	NQ1017-04	−8.12	+1.27
		Muddy dolostone	NQ1018-02	−7.84	+0.49
		Sphalerite-cemented dolostone	NQ1019-01	−9.58	−2.60
		Pale-grey dolostone	NQ1020-01	−10.84	−1.01
		Pale-grey dolostone	NQ1023-01	−7.30	+0.65
	Zebra Dolomite/ankerite	Black dolostone	NQ1017-01	−7.96	+0.57
		Vug-lining ankerite	NQ1017-02	−13.89	−2.61
		Muddy dolostone	NQ1022-01	−9.68	+0.71
		Vug-lining ankerite	NQ1022-02	−11.27	−5.18
	Ankerite	Vug-lining ankerite	NQ1015-02	−13.76	−3.87
		Vug-lining ankerite	NQ1015-03	−14.41	−3.28
		Vug-lining ankerite	NQ1016-01	−13.02	−4.62
		Vug-lining ankerite	NQ1018-01	−14.9	−3.19
		Vug-lining ankerite	NQ1020-02	−11.19	−4.51
		Vug-lining ankerite	NQ1023-02	−10.74	−1.38
Wellheads Hush	Dolomite	Hematised dolostone	NQ1001-02	−7.04	−0.07
		Pale-grey dolostone	NQ1005-01	−9.72	+1.15
		Buff dolostone	NQ1005-02	−9.59	+1.05
		Hematised dolostone	NQ1006-02	−7.28	−0.93
		Pale-grey dolostone	NQ1007-01	−12.00	−7.28
		Hematised dolostone	NQ1008-02	−7.70	−1.95
West Rigg Open Cut	Calcite	Limestone	NQ1043-01	−11.97	+0.21
		Limestone	NQ1045-01	−5.69	−5.26
Eastgate Cement Works Quarry	Dolomite	Hematised dolostone	NQ1025-01	−11.79	−4.83
		Buff dolostone	NQ1026-01	−7.82	−0.60
		Pale-grey dolostone	NQ1027-01	−5.71	−1.77
		Buff dolostone	NQ1028-02	−6.72	−0.75
	Late Calcite	Late coarsely crystalline calcite	NQ1026-03	−11.74	−4.82
		Late coarsely crystalline calcite	NQ1028-01	−10.2	−4.24
Rogerly Mine	Dolomite	Hematised dolostone	NQ1011-01	−7.59	−1.91
		Hematised dolostone	NQ1013-01	−12.99	+1.25
		Hematised dolostone	NQ1014-01	−8.08	−1.75
Hilton Mine	Calcite	Limestone	NQ1039-01	−7.67	−5.67
		Recrystallised Limestone	NQ1041-01	−12.16	−3.34

The host rocks to the stratabound mineralisation are extensively dolomitised/ankeritised with well-developed open porosity in fractures and vugs. Vugs are centimetre to the metre scale, typically elongate parallel to bedding, locally post-date an earlier episode of fracturing and have irregular geometries, which would be highly unlikely to have been generated by fracturing (Fig. 5a).

Host rock replacive dolomite forms inclusion-rich, idiotopic-subhedral mosaics of predominantly non-luminescent crystals, with varying amounts of intercrystalline fines. Relics of primary fabrics including bioclasts in crystal cores are locally preserved. Fe and Mn contents in the earlier generations of dolomite are relatively low (Fig. 3d–f). The cloudy nature of the dolomite and the small sizes of inclusions precluded the acquisition of fluid microchemical data. Limited thermometric data indicate high salinities (18–23 wt%, mean 21 wt% salt equiv.), suppressed T_{fm} (−55 to −35°C) indicative of mixed NaCl–$CaCl_2$ bearing brines, and T_h in the range of 110–130°C. $\delta^{18}O_{PDB}$ and $\delta^{13}C_{PDB}$ ratios are between −12.9 to −5.6‰ and −7.3 to +1.3‰, respectively, with no coherent co-variations observed between the two isotope systems (Table 2 and Fig. 4).

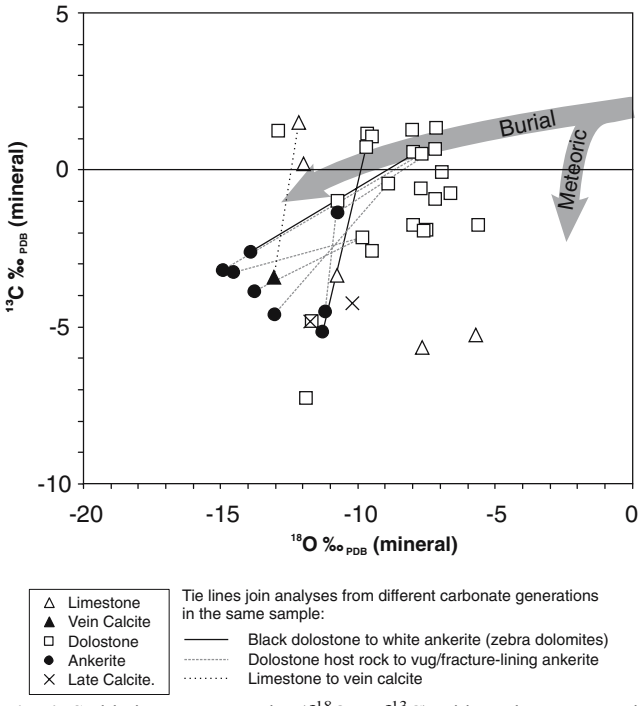

Fig. 4 Stable isotope cross plot (δ^{18}O vs δ^{13}C) with analyses grouped according to location and mineral (calcite, dolomite, etc). For comparative purposes the generalised burial and meteoric diagenetic trends for carbonates are also illustrated (Choquette and James 1987)

The earliest generations of fracture- and vug-lining dolomite are inclusion-poor with idiotopic-euhedral morphologies clearly indicative of growth into open space, but with minor element (Fig. 3) and fluid inclusion chemistries comparable with dolomite in the host rock. Later generations of vein- and vug-lining dolomite become progressively more ferroan and manganoan (to ankerite) with saddle-shaped projections (xenotopic-cement; up to 5 mm) into open-pore space (Fig. 5a). Fluid inclusions in ankerite have similar salinities and T_{fm} temperatures to those in host rock dolomite, indicating a degree of similarity between the fluids responsible for dolomitisation and those responsible for ankerite precipitation. However, T_h are more variable (80–160°C), and there is also a small population of monophase inclusions, which we interpret to represent "stretched" fluids, from the lower end of the observed T_h frequency distribution (Roedder 1985). $\delta^{18}O_{PDB}$ and $\delta^{13}C_{PDB}$ are light (−14.9 to −10.7 and −5.2 to −1.4‰, respectively; Table 2 and Fig. 4) relative to older host rock replacive dolomite. Paired analyses of host rock replacive and pore-filling dolomite/ankerite indicate a shift of 3–7‰.

Zebra dolomites (Arne and Kissin 1989; Wallace et al. 1994; Nielsen et al. 1998; Boni et al. 2000) are observed at a number of localities. These probably represent a special case of mineralised vugs, with alternating sub-parallel, millimetre to centimetre scale, sheet-like structures, of alternating dark-coloured inclusion-rich idiotopic-subhedral

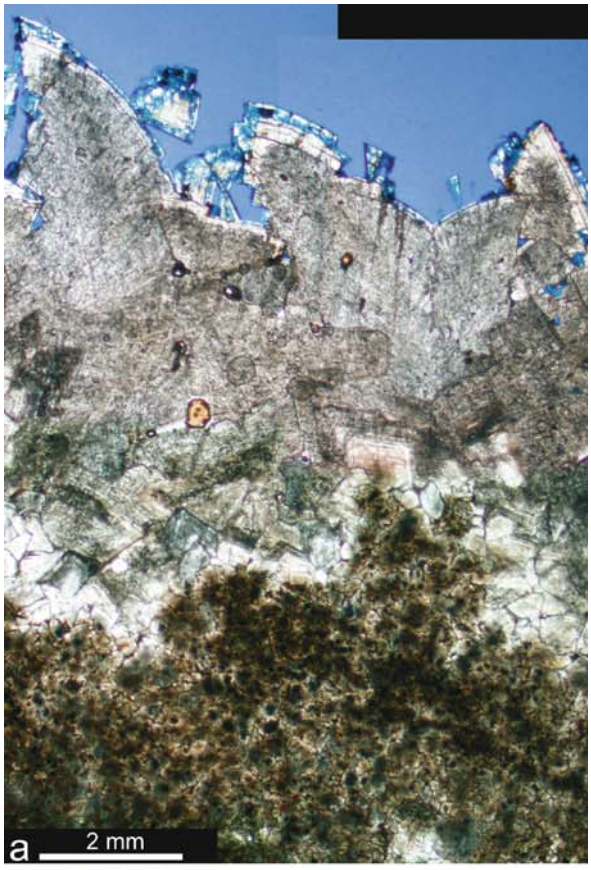

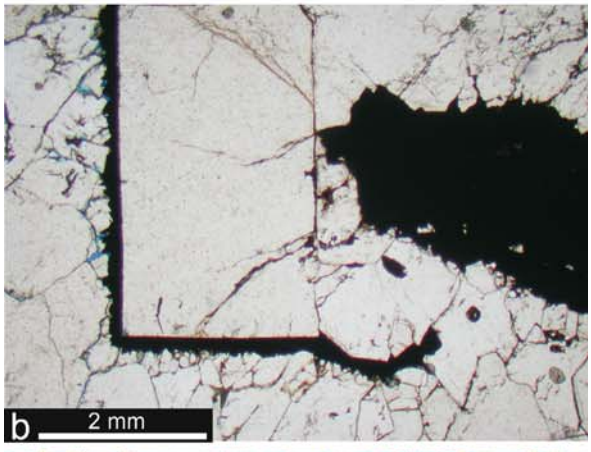

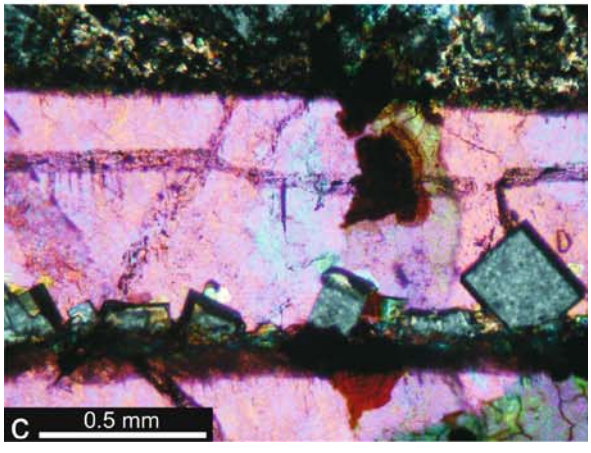

◀ **Fig. 5** **a** Dolostone at the bottom of the image is finely crystalline and inclusion-rich. The vug margin is highly irregular, and the earliest generation of dolomite growing into open pore space is euhedral and relatively inclusion-free. The dolomite becomes progressively coarser-grained, more inclusion-rich, and develops saddle-shaped crystals indicating increasing Fe content (ultimately to ankerite). The outermost generations are lightly corroded. Porosity filled with blue-dyed resin (Small Cleugh Mine; PPL). **b** Fluorite nucleated on an irregular core of (now oxidised) ankerite. A thin band of ankerite, which has subsequently been replaced by Fe- and Mn-oxides is developed on a growth band within the fluorite (Wellheads Hush; PPL). **c** Finely crystalline euhedra (isotropic *grey*) of fluorite on a growth zone within quartz (*pink* birefringent; West Rigg Open Cut; XPL)

dolomite and light-coloured inclusion-poor, xenotopic ankerite. The contacts between the light and dark sheets are in detail irregular or lobate, suggesting that they represent dissolution voids or fractures enhanced by dissolution, rather than simple fractures.

Progressively lighter $\delta^{18}O$ compositions of burial diagenetic carbonate cements are typically attributed to increases in mineral precipitation temperatures (e.g. Choquette and James 1987). However, the degree of isotopic variation seen here implies an increase of ca. 50°C between dolomite and ankerite precipitation, which is not supported by our fluid inclusion data. Therefore, a change in the isotopic composition of the fluid seems a more likely explanation. This is supported by the $\delta^{13}C$ data, which suggest an increased component of CO_2 from organic compounds possibly related to increased hydrocarbon maturation in the source rocks. The progressively higher Fe and Mn contents of dolomite/ankerite are similarly consistent with a progressive shift in fluid composition. In a study of calcite cements on the South Derbyshire platform, Hollis and Walkden (1996) reported similar variations in calcite Fe and Mn contents during mineralisation, which they attributed to progressive clay–mineral transformations in adjacent basins filled with Namurian shales (Boles and Franks 1979) and the reduction of Mn oxide coatings (Francois 1988).

The development of ankerite in vugs indicates that dolomitisation was probably responsible for generation of significant volumes of porosity before mineralisation and, therefore, that dolomitisation played an important role in preparing the ground for stratabound mineralisation. The chemical and isotopic variations suggest that the dolomitising and ankerite-precipitating brines were expelled from progressively maturing basinal shales, possibly over a period extending from the Upper Carboniferous into the early Permian. The high levels of Fe and Mn observed in the later generations of ankerite, may have been sourced from interaction with the Whin Sill (Dunham 1948; Ineson 1968) and/or the Weardale Granite (which in places contains finely divided hematite) during the early stages of hydrothermal circulation in response to extension and fracturing initiated during Late Carboniferous times.

Fluorite–quartz–sulphide mineralisation

There is no simple paragenetic sequence observed, with repeated cycles of fluorite-dominated, quartz-dominated and sulphide-dominated mineralisation observed.

Fluorite lines fractures and vugs and typically engulfs ankerite, although finely crystalline saddle-shaped clusters of ankerite oxidation products trapped on growth bands within fluorite indicate episodic precipitation of ankerite during fluorite precipitation (Fig. 5b). Fluid inclusion T_h span a narrow range (ca.100–120°C; Fig. 2), being notably cooler than most of the published fluid inclusion data for vein mineralisation in the NPO, which typically indicate fluorite precipitation at temperatures in excess of 140°C. (Sawkins 1966; Smith 1974; Moore 1980; Shepherd et al. 1982; Dunham 1990; Christoula 1993; Cann and Banks 2001). Similarly, on the basis of mineral and alkali geothermometry and Eu anomalies in fluorite, the general consensus is that mineralisation occurred from fluids with initial temperatures of at least 220°C (Vaughan and Ixer 1980; Shepherd et al. 1982; Rankin and Graham 1988; Bau et al. 2003; and review in Ixer and Vaughan 1993).

Inclusions in fluorite have high salinities (predominantly >19 wt% salt equiv.), suppressed T_{fm} (−60 to −50°C) , and modelled $NaCl/(NaCl+CaCl_2)$ ratios typically in the range 0.60–0.75 (Fig. 2), although more sodic compositions are noted at the Hilton Mine outlier. The presence of dissolved cations, in addition to Na and Ca, is highlighted by the fact that some inclusions develop an additional K–Fe–Cl daughter phase (composition confirmed during fluid inclusion microchemical analysis). Microchemical analysis of inclusion fluids indicates relatively low K concentrations (typically <7,000 ppm), with correspondingly high Na to K ratios (typically 10:1 to 15:1), which are slightly higher than, but broadly comparable to, values recorded by Rankin and Graham (1988) for crush-leach analyses of fluorite. Microchemical analysis also reveals very high levels of dissolved metals, in particular Fe (Fe up to 7,100 ppm, Cu up to 350 ppm, Zn up to 1,130 ppm and Pb up to 1,200 ppm; Table 3). These values are much greater than those in normal high TDS sedimentary brines. For example, Na–Ca–Cl brines encountered during drilling for hydrocarbons in the central and southern North Sea with similar TDS to the North Pennine inclusions, have typical Fe contents of 50–300 ppm (Warren et al. 1994).

Euhedral *quartz* displays variable paragenetic relationships with fluorite, indicating episodic or cyclic precipitation of fluorite-dominated and quartz-dominated assemblages (Fig. 5c). Fluid inclusions in quartz have similar salinities to those in fluorite (>18 wt% salt equiv.), although modelled compositions are typically more sodic (Fig. 2). Microchemical analyses indicate lower Fe, Cu, Zn and Pb contents and higher Mg and Sr contents than

Table 3 Results of laser-ablation microprobe fluid inclusion microchemical analysis

Sample	Location	Mineral	Estimated Na (ppm)	Li (ppm)	K (ppm)	Mg (ppm)	Mn (ppm)	Fe (ppm)	Cu (ppm)	Zn (ppm)	Sr (ppm)	Ba (ppm)	Pb (ppm)	Na/K wt ratio
NQ1040	Hilton Mine	Barite	50,000[a]	n.a.	40900	1100	n.d.	m.i.	m.i.	m.i.	m.i.	m.i.	m.i.	1.22
			50,000[a]	n.a.	16600	500	n.d.	m.i.	m.i.	m.i.	m.i.	m.i.	m.i.	3.01
			50,000[a]	n.a.	37000	2100	n.d.	m.i.	n.d.	m.i.	m.i.	m.i.	m.i.	1.35
			50,000[a]	n.a.	40100	5900	m.i.	m.i.	m.i.	m.i.	m.i.	m.i.	m.i.	1.25
			50,000[a]	n.a.	20300	3900	m.i.	m.i.	m.i.	m.i.	m.i.	m.i.	m.i.	2.46
			50,000[a]	n.a.	35100	4800	600	m.i.	m.i.	m.i.	m.i.	m.i.	m.i.	1.42
			50,000[a]	n.a.	37000	5600	n.d.	m.i.	m.i.	m.i.	m.i.	m.i.	m.i.	1.35
			50,000[a]	n.a.	15800	m.i.	m.i.	m.i.	n.d.	m.i.	m.i.	m.i.	m.i.	3.16
			50,000[a]	n.a.	32500	7600	m.i.	m.i.	m.i.	m.i.	m.i.	m.i.	m.i.	1.54
			50,000[a]	n.a.	38200	10300	m.i.	m.i.	m.i.	m.i.	m.i.	m.i.	m.i.	1.31
			50,000[a]	n.a.	4000	1100	300	m.i.	m.i.	m.i.	m.i.	m.i.	m.i.	12.50
		Fluorite	65 000	320	5900	720	250	n.d.	n.d.	n.d.	660	2100	200	11.02
			65 000	n.d.	4900	n.d.	n.d.	n.d.	n.d.	n.d.	180	400	n.d.	13.27
			65 000	200	4000	580	120	7100	350	m.i.	700	n.d.	n.d.	16.25
			65 000	220	4300	430	80	1200	10	10	350	140	n.d.	15.12
			65 000	n.d.	3800	830	n.d.	3600	110	n.d.	550	n.d.	10	17.11
NQ1011	Rogerly Mine	Fluorite	60 000	150	7000	1000	90	620	50	120	410	90	20	8.57
			60 000	90	5700	1300	200	2400	180	450	360	770	1200	10.53
			60 000	90	7200	1600	610	m.i	310	1130	510	250	1200	8.33
		Quartz	60 000	1800	3500	900	100	n.d.	n.d.	n.d.	360	60	90	17.14
			60 000	90	3000	300	n.d.	n.d.	n.d.	n.d.	270	70	n.d.	20.00
NQ1021	Smallcleugh Mine	Quartz	75,000[a]	n.a.	5700	3400	130	1200	20	80	1500	190	60	13.60
			75,000[a]	n.a.	18900	6100	m.i.	m.i.	n.d.	710	330	m.i.	470	4.10
			75,000[a]	n.a.	22500	1400	60	m.i.	n.d.	40	2200	70	30	3.44
			75,000[a]	n.a.	17800	m.i.	m.i.	m.i.	50	m.i.	m.i.	m.i.	n.d.	4.35
			75,000[a]	n.a.	5000	400	70	80	n.d.	20	820	60	20	15.50
			75,000[a]	n.a.	6100	1700	100	590	n.d.	140	1300	60	60	12.70
			75,000[a]	n.a.	6200	1500	20	870	n.d.	40	560	40	n.d.	12.50
			75,000[a]	n.a.	24200	1200	40	170	n.d.	20	1200	90	10	3.20

Concentrations are determined relative to Na concentrations, which are known from fluid inclusion microthermometric analysis.
n.a. Not analysed, *n.d.* not detected, *m.i.* matrix interference prevented concentration determination
[a] Analyses were run using a dynamic reaction cell (see "Materials and methods section").

inclusions in fluorite (Table 3). Some inclusions have Na to K ratios comparable to those present in fluorite (approximate range 10:1 to 20:1), whereas others have low Na/K ratios (approximate range 3:1 to 5:1), with a closer affinity to inclusions in barite (see below). There is also a small, but significant, population of relatively low-salinity inclusions (<10 wt% salt equiv.; Fig. 2).

T_h are comparable with fluorite (typically 90–130°C; Fig. 2), but there is also a small population of monophase inclusions, which may indicate that quartz precipitation continued at lower temperatures than those that prevailed during fluorite precipitation. There is no relationship between inclusion type (monophase vs two-phase) and salinity. These temperatures are notably lower than those reported in earlier studies, which are typically in the range 120–200°C (Smith 1974; Moore 1980; Christoula 1993; Fig. 2).

Sulphides A full description of the sulphide minerals and their relationships is outside the scope of this study, but summaries can be found in Vaughan and Ixer (1980) and Dunham (1990). The sulphide mineralogy of the stratabound mineralisation studied here is dominated by galena and sphalerite, although minor pyrite and chalcopyrite are also noted. Sulphides occur predominantly as vein- or vug-filling euhedra with minor amounts also present in the wall rocks. There are numerous examples of sulphide precipitation beginning approximately coeval with the onset of fluorite precipitation. However, fluorite precipitation continued after sulphide precipitation stopped. Limited fluid inclusion data from sphalerite indicate high salinities (21–23 wt% NaCl equiv.) and highly variable T_h (80–150°C; Fig. 2).

Calcite Minor calcite tends to occur as veins or cement within brecciated domains and is characterised by notably higher Fe and Mn contents and lower Mg contents (Fig. 3) than the calcite in the host rocks and in later supergene calcite.

Petrographic and field observations indicate that, rather than representing exclusively metasomatic replacement of the host rocks, the fluorite–quartz–sulphide mineralisation occurred in a structurally active setting. *Mineralised breccias*, where earlier minerals are brecciated and recemented by later mineralisation, are particularly common and may be poly-mineralic (Fig. 6a) or mono-mineralic (Fig. 6b). Rare examples of *internal sediments* are also observed. Here, mineralised cavities are lined by laminae (1 to 2 mm thick) of fine-grained Fe and Mn oxides (oxidation products of ankerite) and irregular fluorite and quartz crystals, cemented by finely crystalline quartz and fluorite. Contemporaneity of the sediment relative to the mineralisation is locally demonstrated where the sediment lies on top of a fracture or vug-coating of fluorite, and, in turn, is overlain by coarsely crystalline fluorite (Fig. 6c). These sediments display faint internal lamination, which thicken into irregular surfaces on fracture/vug margins (Fig. 6d).

Furthermore, there is evidence for modification and enhancement of the existing fracture and vuggy pore system during mineralisation. A degree of dissolution of carbonate wall rock would be expected in response to the reduction in fluid pH that would occur as metal sulphides are precipitated from a chloride-rich solution. Models of mixing between brine and a low-salinity groundwater in carbonate host rock (Corbella et al. 2004) appear to provide a satisfactory explanation for the observed redistribution of porosity during mineralisation.

The generally accepted models for generation of the NPO invoke mineralisation in response to mixing of fluoride-rich, metalliferous brines with low-salinity surficial or connate brines (e.g. Solomon et al. 1971; Cann and Banks 2001). However, to our knowledge, direct evidence of a low-salinity component has not previously been demonstrated. By investigating the stratabound mineralisation marginal to the veins, we have been able to sample the low-salinity component, and these results lend support to models of mineralisation in response to fluid mixing. We suggest that the sources of the two fluids are:

1. The low-salinity component possibly represents groundwater that percolated through the Lower Carboniferous sediments during Latest Carboniferous and Permian unroofing of the NPO.
2. The high-salinity component could be derived from dense evaporated brines generated during the Late Permian in the adjacent Zechstein Sea and Vale of Eden Basins (Cann and Banks 2001). Cann and Banks (2001) also suggested that a major factor, which governed the timing of the mineralisation, was the temporally restricted occurrence of high-salinity brines to Late Permian times. As postulated by Cann and Banks (2001), these brines would have percolated to great depth through fractures generated during Permian extension, into a hydrothermal convection cell associated with the high heat production Weardale Granite. At these depths, the fluids could become heated and might be expected to react with both the Palaeozoic basement and the granite along their flow paths, which probably accounts for their high fluorine and highly elevated metal contents, before being driven back upwards into the fracture system above the granite where mixing and mineralisation occurred.

The preferential preservation of the low-salinity fluid in quartz, coupled with the more sodic compositions of the inclusions in quartz, suggests that quartz precipitation is more strongly associated with the lower-salinity fluid than the fluorite, possibly reflecting the waning stages of

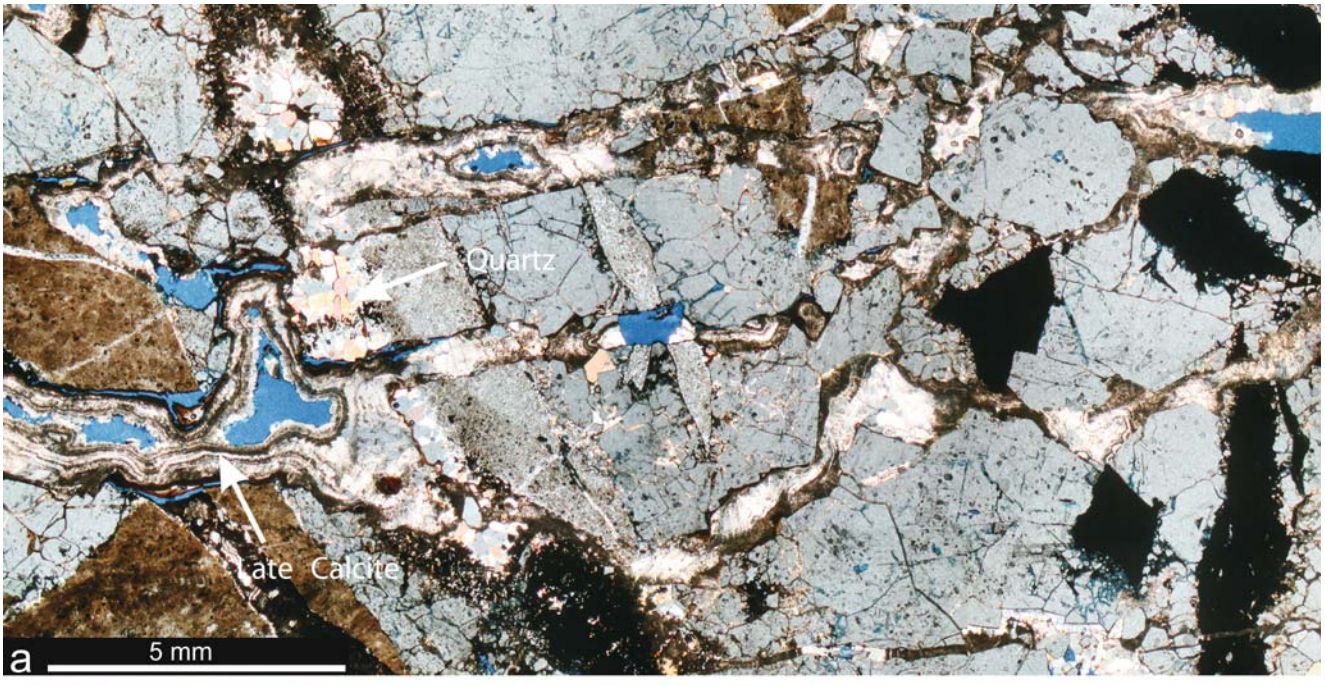
Quartz
Late Calcite
a
5 mm

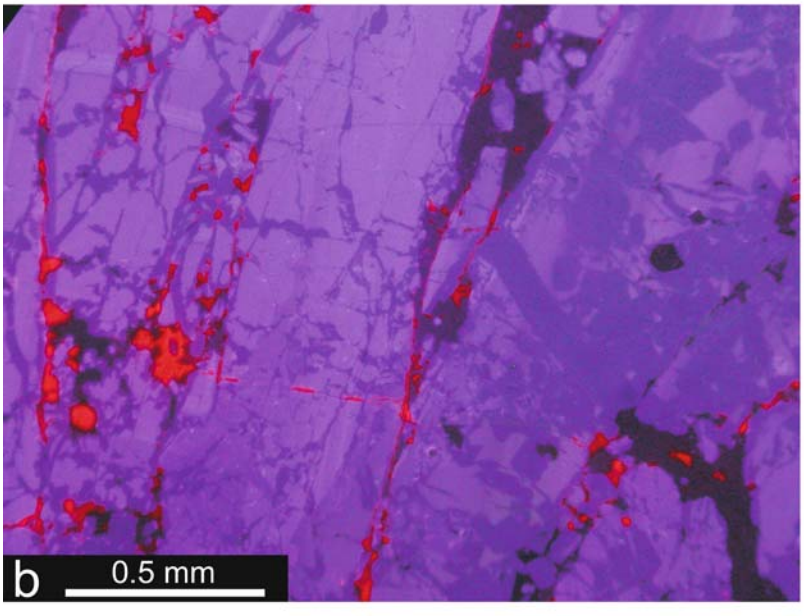
b
0.5 mm

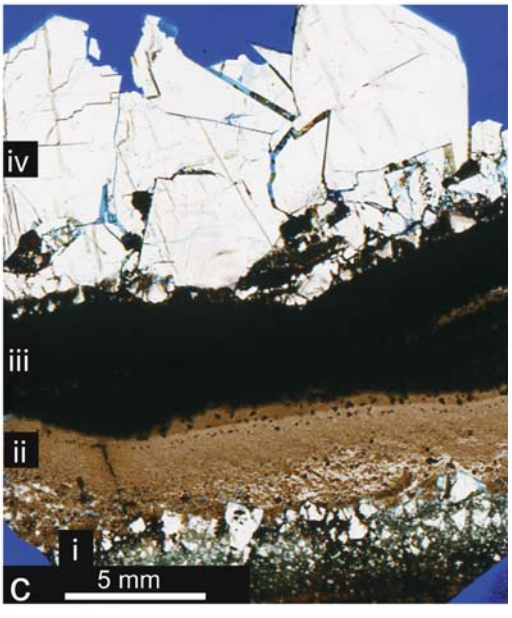
iv
iii
ii
i
c
5 mm

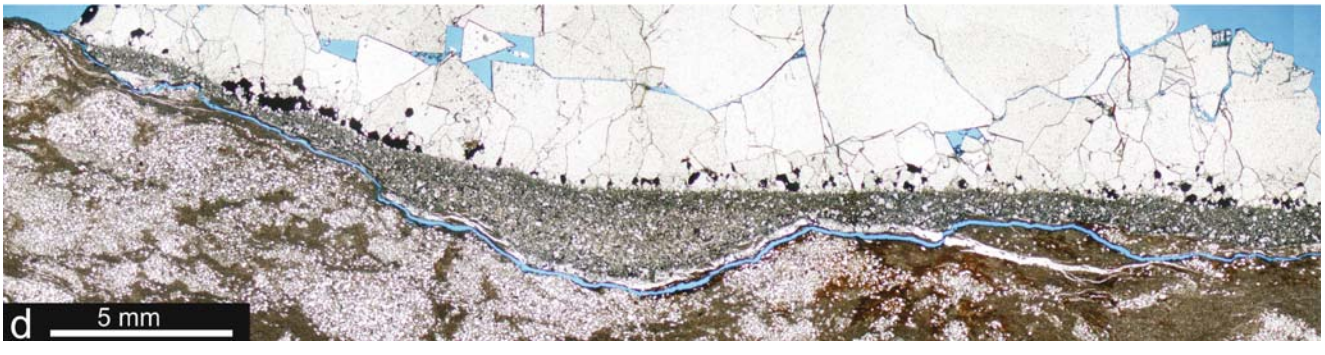
d
5 mm

◀ **Fig. 6** **a** Coarsely crystalline fluorite (*grey*) is extensively brecciated and recemented by patches of quartz (*arrowed*) and late finely crystalline, banded calcite (*arrowed*; West Rigg Open Cut, XPL). **b** Fluorite showing variations in luminescence between successive fluorite generations. Earlier generations are brecciated and recemented by later fluorite. Later microfractures are cemented by red-luminescent smithsonite (Eastgate Cement Works Quarry, CL). (**c**) Scan of polished thin-section showing (*i*) a relatively early substrate comprising brecciated fluorite. On top of this is developed (*ii*) a finely cross-laminated internal sediment of fine-grained irregularly crystalline fluorite and carbonate grains cemented by silica. This is overlain by (*iii*) a band of opaque oxidised ankerite, and finally by (*iv*) coarsely crystalline fluorite (Eastgate cement works quarry). **d** A shaley host rock with an irregular surface upon which are deposited finely laminated internal sediments which thicken into the hollows. On top of the internal sediment are developed finely crystalline galena euhedra (opaque, *black*), which are engulfed by fluorite (*white*). A thin smithsonite vein exploits the plane of weakness between the host rock and the internal sediment (Hilton Mine, PPL)

individual influxes of metalliferous brines. This interpretation is also supported by the fluid inclusion microchemical data, with inclusions in fluorite having variable but elevated levels of metals, whereas metal contents in quartz are significantly lower. The lack of direct evidence for the low-salinity fluid in the main vein mineralisation may not be surprising as the stratabound mineralisation is distal relative to the fault-controlled migration pathways of the mineralising fluid. Consequently, the stratabound mineralisation might be expected to retain a greater signature of the pre-mineralisation pore fluids.

Barium mineralisation

Barite is only observed in our samples from the mineralised outlier at Hilton Mine, where it forms radial bundles of tabular crystals engulfing vug-lining, euhedral fluorite. Fluid inclusions are overwhelmingly monophase, indicating relatively cool conditions during precipitation. Salinities are relatively low (typically 15 to 20 wt% salt equiv.), and a very low salinity component (<5 wt% salt equiv.) is also observed (also reported by Cann and Banks 2001). Suppressed T_{fm} (ca. −55°C) suggest that a mixed NaCl–$CaCl_2$ brine characterised by relatively low Na to K ratios (typically 1:1 to 3:1; Table 3), which are comparable with those of highly evaporated marine waters (Timofeeff et al. 2001), was responsible for barite precipitation.

We have no new stable isotope data for barite. However, published $\delta^{34}S$ and $\delta^{18}O_{SMOW}$ data are consistent with sulphate derived from Triassic brines or Lower Carboniferous seawater (Solomon et al. 1971) or from Lower Carboniferous evaporites in the Northumberland-Solway Basin (Crowley et al. 1997). $\delta^{18}O_{SMOW}$ are predominantly between 10 and 15‰ and, assuming barite crystallisation occurred at relatively low temperatures (ca. 50°C) as suggested by the monophase nature of the fluid inclusions, this equates to a fluid with $\delta^{18}O_{SMOW}$ in the range −13 to −7‰ (using the fractionation factors of Friedman and O'Neil 1977). This is notably lighter than the fluid responsible for dolomite and ankerite precipitation suggested by our $\delta^{18}O$ and T_h data (−2.2 to +5.4 and −4.2 to +0.1‰, respectively). The lower temperatures and salinities of fluid inclusions in barite relative to inclusions in fluorite and quartz may indicate that barite deposition represents the waning stages of hydrothermal circulation, possibly under slightly cooler conditions when the sources of metals within the basement and/or igneous intrusions had become depleted.

Conclusions

By looking into the relatively distal portions of the NPO mineralisation system, we have been able to demonstrate the involvement of a number of different fluids in its evolution and genesis. Previous models for the genesis of the NPO have invoked mixing of high-temperature, high-salinity, fluoride-rich, metalliferous brines with low-salinity, sulphate-bearing brines (e.g. Solomon et al. 1971; Cann and Banks 2001). Our data confirm this model and also provide the first direct confirmation of the presence of the low-salinity component within the central fluorite zone. Furthermore, the metal contents of the high salinity component are very high, relative to normal high TDS basinal brines. This indicates that this fluid was probably modified through interaction with the Weardale Granite, the Whin Sill and/or the Palaeozoic basement during hydrothermal circulation.

The stratabound mineralisation in the NPO was generally considered as a passive, metasomatic replacement adjacent to the main vein mineralisation. This study demonstrates the importance of dolomitisation in generating significant proportions of porosity, which host the stratabound mineralisation, and also indicates that significant brecciation and dissolution accompanied the mineralisation.

The extensive stratabound mineralisation within the Great Limestone at Boltsburn (Weardale) and Allenheads (East Allendale) mines (Fig. 1) constituted two of Britain's largest and most productive lead ore bodies. Similar deposits, also within the Great Limestone, yielded large tonnages of both lead and zinc ores at several mines in the Nenthead area. Stratigraphically lower limestones were generally little explored in the NPO, although, where such exploration has occurred, significant mineralisation was found, notably within the Tynebottom Limestone at Rotherhope Fell Mine, near Alston. The discovery of zinc-rich mineralisation in even lower limestones in the Rookhope Borehole (Dunham et al. 1965) and in the deepest workings of Cambokeels Mine, Weardale, may point to significant potential for economic stratabound mineralisation at depth.

Acknowledgements The authors wish to thank numerous colleagues who have provided valuable technical support throughout this study. David Banks and Linda Berry, University of Leeds, are thanked for assistance given to TJS during the laser ablation fluid inclusion microchemical analyses. We also wish to thank the reviewers Volker Leuders and Bernd Lehman for constructive reviews, which helped clarify the focus of this paper. Publication for JEB, JN, AB, JAM and BY is by permission of the Directory, British Geological Survey, NERC.

References

Allan MM, Yardley BWD, Forbes LJ, Shmulovich KI, Banks DA, Shepherd TJ (2006) Validation of LA-ICP-MS fluid inclusion analysis with synthetic inclusions. Am Mineral 90:11–12

Arne DC, Kissin SA (1989) The significance of "diagenetic crystallization rhythmites" at the Nanisivik Pb–Zn–Ag deposit, Baffin island, Canada. Miner Depos 24:230–232

Bau M, Romer RL, Lüders V, Dulski P (2003) Tracing element sources of hydrothermal mineral deposits: REE and Y distribution and Sr–Nd–Pb isotopes in fluorite from MVT deposits in the Pennine Orefield, England. Miner Depos 38:992–1008

Boles JR, Franks SG (1979) Clay diagenesis in Wilcox sandstones of Southwest Texas; implications of smectite diagenesis on sandstone cementation. J Sediment Petrol 49:55–70

Boni M, Parente G, Bechstadt T, De Vivo B, Iannace A (2000) Hydrothermal dolomites in SW Sardinia (Italy): evidence for a widespread late-Variscan fluid flow event. Sediment Geol 131:181–200

Bruckschen P, Veizer J (1997) Oxygen and carbon isotopic composition of Dinantian brachiopods: Paleoenvironmental implications for the Lower Carboniferous of western Europe. Palaeogeogr Palaeoclimatol Palaeoecol 132:243–264

Cann JR, Banks DA (2001) Constraints on the genesis of the mineralization of the Alston Block, Northern Pennine Orefield, northern England. Proc Yorks Geol Soc 53:187–196

Choquette PW, James NP (1987) Diagenesis 12. Diagenesis in limestones 3. The deep burial environment. Geosci Can 14:3–35

Christoula M (1993) Fluid inclusion geochemistry of selected epigenetic, low temperature mineralization in the U.K. Ph.D. Thesis, Imperial College of Science and Technology, London University

Corbella M, Ayora C, Cardellach E (2004) Hydrothermal mixing, carbonate dissolution and sulfide precipitation in Mississippi Valley-type deposits. Miner Depos 39:344–357

Crowley SF, Bottrell SH, McCarthy MDB, Ward J, Young B (1997) delta S-34 of lower Carboniferous anhydrite, Cumbria and its implications for barite mineralization in northern Pennines. J Geol Soc 154:597–600

Davison JM, Ineson PR, Mitchell JG (1992) Potassium–argon isotope age determinations from the metasomatic alteration of the Great Limestone, Northern Pennine Orefield. Proc Yorks Geol Soc 49:71–74

Dunham KC (1948) Geology of the Northern Pennine Orefield, vol. 1. Tyne to Stainmore, 1st edn. Memoir of the Geological Survey of Great Britain. HMSO, London

Dunham KC (1990) Geology of the Northern Pennine Orefield, vol. 1. Tyne to Stainmore. Economic memoir covering the areas of 1:50000 and one-inch geological sheets 19 and 25 and parts of 13, 24, 26, 31, 32 (England and Wales) British Geological Survey. HMSO, London, p 299

Dunham KC, Wilson AA (1985) Geology of the Northern Pennine Orefield, vol. 2. Stainmore to Craven. Memoir of the Geological Survey of Great Britain. HMSO, London

Dunham KC, Dunham AC, Hodge BL, Johnson GAL (1965) Granite beneath Viséan sediments with mineralization at Rookhope, northern Pennines. J Geol Soc 121:383–417

Dunham KC, Fitch FJ, Ineson PR, Miller JA, Mitchell JG (1968) The geochronological significance of argon-40/ argon-39 age determinations on White Whin from the northern Pennine orefield. Proc R Soc Lond A Math Phys Sci 307:251–266

Fitch FJ, Miller JA (1967) The age of the Whin sill. Geol J 5:233–250

Francois R (1988) A study on the regulation of the concentrations of some trace metals (Rb, Sr, Zn, Pb, Cu, V, Cr, Ni, Mn and Mo) in Saanich Inlet sediments, British Columbia, Canada. Mar Geol 83:285–308

Friedman I, O'Neil JR (1977) Compilation of stable isotope fractionation factors of geochemical interest. USGS Prof Pap 440-KK

Goldstein RH (2001) Fluid inclusions in sedimentary and diagenetic systems. Lithos 55:159–193

Gunther D, Frischknecht R, Heinrich CA, Kahlert HJ (1997a) Capabilities of an Argon Fluoride 193 nm excimer laser for laser ablation inductively coupled plasma mass spectrometry microanalysis of geological materials. J Anal At Spectrom 12:939–944

Gunther D, Frischknecht R, Muschenborn HJ, Heinrich CA (1997b) Direct liquid ablation: a new calibration strategy for laser ablation ICP-MS microanalysis of solids and liquids. Fresenius' J Anal Chem 359:390–393

Hollis C, Walkden G (1996) The use of burial diagenetic calcite cements to determine the controls upon hydrocarbon emplacement and mineralization on a carbonate platform, Derbyshire, England. In: Strogen P, Somerville ID, Jones GLL (eds) Recent advances in lower carboniferous geology. Geol Soc Lond Spec Pub 107:35–49

Ineson PR (1968) The petrology and geochemistry of altered quartz–dolerite in the Closehouse Mine area. Proc Yorks Geol Soc 36:373–384

Ixer RA (1986) The ore mineralogy and paragenesis of the lead–zinc–fluorite–barite orefields of the English Pennines and Mendip Hills. In: Craig JR (ed) Mineral parageneses. Theophrastus, Athens, pp 179–211

Ixer RA, Vaughan DJ (1993) Lead–zinc–fluorite–baryte deposits of the Pennines, North Wales and the Mendips. In: Pattrick RAD, Polya DA (eds) Mineralization in the British Isles. Chapman & Hall, London, pp 355–418

Ixer RA, Young B, Stanley CJ (1996) Bismuth-bearing assemblages from the Northern Pennine Orefield. Min Mag 60:317–324

Lenehan T (1997) An investigation into thermo-tectonic and maturation histories in north-west Britain. Ph.D. Thesis, University of Leeds

McCrea J (1950) On the isotopic chemistry of carbonates and palaeotemperature scale. J Chem Phys 18:849–857

Moore GR (1980) A chemical and isotopic study of fluid inclusions from the Northern Pennine Orefield. Ph.D. Thesis, Durham University

Naden J (1996) CalcicBrine 1.5: a Microsoft Excel 5.0 add-in for calculating salinities from microthermometric data in the system NaCl–$CaCl_2$–H_2O. PACROFI VI Abstracts. University of Wisconsin

Nielsen P, Swennen R, Muchez P, Keppens E (1998) Origin of Dinantian zebra dolomites south of the Brabant-Wales Massif, Belgium. Sedimentology 45:727–743

Plant J, Jones D, Smith N, Shepherd T (1995) Carboniferous shale basins as sources of Pennine ore fluids: implications for MVT ore deposit formation. In: Pasava J, Kribek B, Zak K (eds) Mineral deposits: their origin to their environmental impacts. A.A. Balkema, Rotterdam, pp 967–970

Rankin AH, Graham MJ (1988) Na, K and Li contents of mineralizing fluids in the Northern Pennine Orefield, England and their genetic significance. Trans Inst Min Metall B Appl Earth Sci 97:99–107

Roedder E (1985) Fluid inclusions. Mineral Soc Am Rev Miner 12:644

Rosenbaum J, Sheppard SMF (1986) An isotopic study of siderites, dolomites and ankerites at high temperatures. Geochim Cosmochim Acta 50:1147–1150

Sawkins FJ (1966) Ore genesis in the North Pennine orefield, in the light of fluid inclusion studies. Econ Geol 61:385–401

Shepherd TJ, Darbyshire DPF, Moore GR, Greenwood DA (1982) Rare earth element and isotopic geochemistry of the North Pennine ore deposits. In: Anonymous (ed) Symposium Jules Agard; Gites filoniens Pb–Zn–F–Ba de basse temperature du domaine varisque d'Europe et d'Afrique du Nord; III, Etudes geochimiques et modeles genetiques; etudes structurales; Guide de prospection. Bureau de Recherches Geologiques et Minieres, (BRGM), Paris, France, pp 371–377

Smith FW (1974) Factors governing the development of fluorspar orebodies in the North Pennine Orefield. Ph.D. Thesis, Durham University, p 395

Solomon M, Rafter TA, Dunham KC (1971) Sulphur and oxygen isotope studies in the northern Pennines in relation to ore genesis. Trans Inst Min Metall B Appl Earth Sci 80:259–275

Solomon M, Rafter TA, Dunham K (1972) Sulphur and oxygen isotope studies in the northern Pennines in relation to ore genesis; discussion. Trans Inst Min Metall B Appl Earth Sci 81:172–177

Timofeeff MN, Lowenstein TK, Brennan ST, Demicco RV, Zimmermann H, Horita J, von Borstel LE (2001) Evaluating seawater chemistry from fluid inclusions in halite: Examples from modern marine and nonmarine environments. Geochim Cosmochim Acta 65:2293–2300

Tucker M, Wright VP (1990) Carbonate sedimentology. Blackwell Scientific, p 482

Vaughan DJ, Ixer RA (1980) Studies of sulphide mineralogy of North Pennine ores and its contribution to genetic models. Trans Inst Min Metall B Appl Earth Sci 89:99–109

Wallace MW, Both RA, Ruano SM, Fenoll HAP, Lees T (1994) Zebra textures from carbonate-hosted sulfide deposits; sheet cavity networks produced by fracture and solution enlargement. Econ Geol 89:1183–1191

Warren E, Smalley P, Howarth R (1994) Part 4: Compositional variations of North Sea formation waters. In: Warren E, Smalley P (eds) North Sea formation waters atlas. Blackwell [for the] Geological Society of London, London, pp 119–206

Young B, Styles MT, Berridge NG (1985) Niccolite–magnetite mineralization from Upper Teesdale, North Pennines. Min Mag 49:555–559